An Atomistic Modeling and Quantum Mechanical Approach to the Hydrolytic Degradation of Aliphatic Polyesters

María Entrialgo-Castaño,[1] *Anthony E. Salvucci,*[2] *Andreas Lendlein,*[1] *Dieter Hofmann**[1]

Summary: This paper reports computational simulations at two different scales employed to investigate the hydrolytic degradation of two homopolyesters: polyglycolide, PGA and poly(*L*-lactide), PLLA. Atomistic bulk models were used to investigate the dry and various hydrated states of the two systems. In addition, the first moments of contact between the polymers and water were studied employing atomistic interface models. A higher affinity of water to polyglycolide in comparison with poly(*L*-lactide) was observed, while diffusion of water was found to be lower in the first polymer. Quantum chemical calculations for the first step of the water-assisted hydrolysis revealed a higher resistance to hydrolytical scission of the *L*-lactyl units in comparison to glycolyl units.

Keywords: aliphatic polyesters; free volume; hydrolytic degradation; molecular modeling; quantum chemical calculations

Introduction

Aliphatic poly(α-hydroxy esters) derived from glycolic and lactic acid have been widely studied and long utilized as synthetic degradable biomaterials[1–4] for fracture fixations, interference screws, suture anchors, craniomaxillofacial fixation and meniscus repair.[5] Furthermore, they have been broadly investigated for gene and drug delivery[6] and have been employed in the development of biodegradable shape-memory polymeric networks, with a high potential for new applications in the field of minimally invasive surgery.[7,8] Although enzymatic processes play an important role in the degradation of these aliphatic polyesters in animals (i.e. rabbits), it is considered to occur primarily via a hydrolytic mechanism in humans.[9] The degradation of these polyesters leads to glycolic and lactic acid, which can be either directly excreted or further metabolized into carbon dioxide and water, and then excreted afterwards.[10]

The importance of regulation of the degradation rate and type of these biomaterials for the above mentioned applications is undeniable, and yet, the main factors governing the process are, unfortunately, not entirely understood. This knowledge is essential in attaining effective control over their degradation behavior, which is highly desired. Experimental work carried out to elucidate the basic phenomena involved in the hydrolytic degradation and erosion of polyesters over the last decades has delivered important information.[11] However, an even more profound understanding of the mechanism of degradation can be achieved by combining this information with insight into the basic processes at an atomistic level. This insight is difficult to access via experimental techniques, but can be obtained using simulation techniques, such as computer assisted molecular modeling

[1] GKSS Research Center, Institute of Polymer Research, Kantstrasse 55, 14513 Teltow, Germany
Fax: (+49) 3328 352 452;
E-mail: dieter.hofmann@gkss.de
[2] Department of Biological and Environmental Engineering, Riley-Robb Hall, Cornell University, Ithaca, NY 14853

and quantum chemical calculations. These two computational techniques provide additional, valuable information about structure-property relationships. Therefore, they are most suitable for the study of degradation of polymers because the complex process of hydrolytic degradation is a transport-reaction mechanism, encompassing the transport of water in the polymer, the hydrolytic cleavage of the bonds of cahain, the transport of degradation products and their subsequent absorption in the surrounding media. Molecular dynamics and quantum mechanical calculations permit examination into these fundamental processes of uptake, permeation of individual water molecules into the materials and the scission of the individual bonds. For our investigation, we have selected the two homopolyesters of the lactide/glycolide family, polyglycolide, and poly(*L*-lactide), It has previously been reported[4,5,12–15] that both water uptake and weight loss are faster for polyglycolide than for poly(*L*-lactide). Both homopolymers are semicrystalline. However, it was established that degradation of these semicrystalline aliphatic polyesters occurs first and predominantly in the amorphous regions, accompanied by an increase of relative crystallinity in the material.[3,16]

In a prior study,[17] we examined the important basic mechanism of water permeation through the aforementioned biomaterials utilizing molecular dynamic (MD) simulations of amorphous bulk models. These models embody the characteristic features of the interior regions of an amorphous polymer. Differences between PGA and PLLA were discussed in relation to the experimentally observed differences in water uptake. Such differences included free volume distribution, mobilities of polymer chain segments and water molecules, and specific energetic interactions between the respective polymer and water molecules. In the present paper, most notably results of quantum chemical investigations and the outcome of atomistic interface simulations, in the early stages of water sorption at the polymer surface, are reported. Since the latter models permit the following of these processes only for a few nanoseconds, bulk models are necessary to model experimental water soaking, which characteristically takes place at much longer times (days and weeks). For this reason, bulk models will be reconsidered in this paper.

Modeling Details

Atomistic Simulations: Bulk Models

Amorphous bulk and interface models were generated using the *Builder*, *Polymerizer* and *Amorphous Cell* modules of the *InsightII/Discover Software* (Accelrys Inc.).[18,19] The basic techniques for the packing and equilibration of the models are described elsewhere.[20] Three independent, amorphous bulk models were constructed for each of the homopolymers, polyglycolide and poly(*L*-lactide). The general parameters for these models, as well as some related experimentally measured properties, are listed in Table 1. Each polymeric chain is constituted of 50 repeat units. The equilibration of the constructed cells consisted of several stages. First, a scaling of the parameters of the forcefield for the torsion terms and the nonbond interactions (Coulomb and Van der Waals) was carried out. Details for this scaling are described by Hofmann et al.[20] Afterwards, a short annealing was performed, consisting

Table 1.
General bulk models parameters and experimental properties.

Polymer Packing	No. of chains/model	No. of atoms/model	Initial packing density (g/cm^3)	Experimental density (g/cm^3)	Experimental Tg (°C)
PGA	21	6342	1.50	1.45[21] (amorphous) 1.50[22] (amorphous)	35–40[1,5]
PLLA	19	8588	1.25	1.24–1.30[23]	60–65[1,5]

of 20 ps NVT–MD (canonical ensemble, where the number of atoms N, the volume V and the temperature T are conserved) at 600 K and followed by 320 ps at 300 K. At this point, the models were subjected to a first density check typically consisting of 40 ps NPT–MD (isothermal-isobaric ensemble, where the number of atoms N, the pressure P and the temperature T are conserved) at 300 K. In cases when these simulations crashed, due to an energy difference between two successive steps larger than the deviation allowed, or when the system was not relaxing at the experimental density, compression to the experimental density – via NPT–MD at a suitable pressure – was carried out. This was followed by an annealing procedure consisting of 20 ps NVT–MD (for each temperature) at 750, 600 and 450 K and finishing with up to 300 ps at 300 K. The last step consisted of at least 1 ns (in most cases 2 ns) NPT–MD at a pressure of 1 bar and a temperature of 310 K. This run was used for the production of data. The temperature was controlled using the *Berendsen*[21] or *velocity scaling method* with a temperature window of 10 K. In the NPT–MD runs, the pressure was controlled using the *Berendsen* barostat.[21] During the simulations, a group based summation method for the nonbond interactions was employed (in the first step of the equilibration, the *cell multipole method* for the treatment of the nonbond interactions was used) with a cutoff of 18 Å.

Bulk models were constructed using two different force fields: the COMPASS[25] forcefield and the polymer consistent forcefield, PCFF, modified by Blomqvist et al.[26,27] The evaluation and selection of the best suitable forcefield, by comparison with experimental densities and experimental X-ray scattering curves, was published in a previous paper.[17] Supplementary evaluation of the forcefields was done by analyzing torsional statistics and comparing the resulting distributions with quantum chemical results reported by Blomqvist et al.[26] The selected dihedral angles, as displayed in Figure 1, were monitored every 1 ps during NPT–MD dynamics up to 100 ps. The dihedral angle involving the backbone atoms C1–O2–C3–C4 was labeled O2–C3 (Figure 1a), and the angle involving the backbone atoms O2–C3–C4–O5 was labeled C3–C4 (Figure 1b).

The distribution of values for the two selected dihedral angles in both polymers using the COMPASS forcefield is shown in Figure 2. The respective distributions of dihedrals for the models created with the modified PCFF force field are shown in Figure 3. For the O2-C3 torsion of a molecule consisting of two glycolic acid repeat units, Blomqvist et al. found, at the MP2 quantum mechanical calculation level, a high *cis* energy barrier (0 °), a lower rotational barrier around 140–150 °, a global energy minimum at 74.3 ° and a smaller minimum at 180 °.[26] This torsion potential is symmetric around the *cis* conformation.

Because Figure 2 and 3 show frequencies of conformation angles, a comparison with the energy profiles reported in reference [26] needs to consider that these two situations are inverse to each other, i.e. an energy maximum in reference [26] corresponds to a minimum of conformation angle frequency and vice-versa.

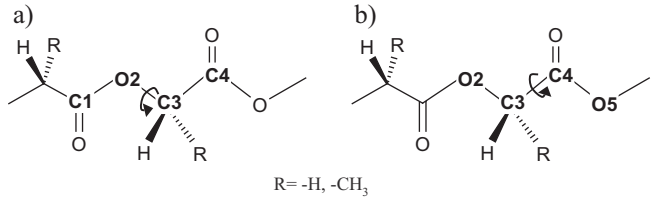

Figure 1.
Definition of the analyzed dihedral angles (a) dihedral O2–C3 (b) dihedral C3–C4.

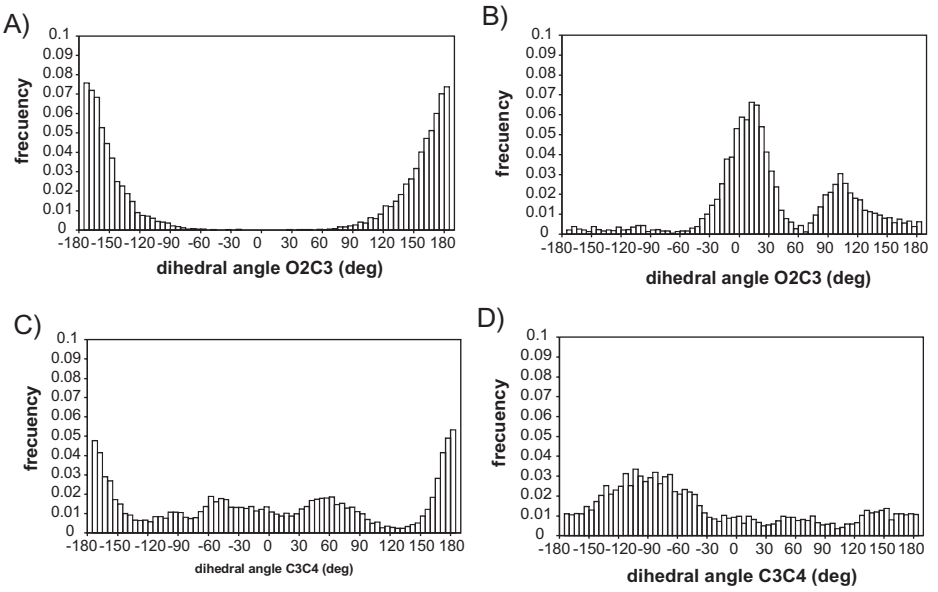

Figure 2.
Distribution of values obtained for the selected dihedral angles using the COMPASS forcefield. Graphs A and C: PGA; Graphs B and D: PLLA.

The distribution for the O2–C3 dihedrals calculated using the COMPASS forcefield (see Figure 2A) shows only one maximum at 180° (which would correspond to a torsional potential minimum), but there is no global maximum of dihedral angle frequency at about 75°, which would correspond to the respective MP2 energy minimum. However, the models of PGA constructed using the modified PCFF for-

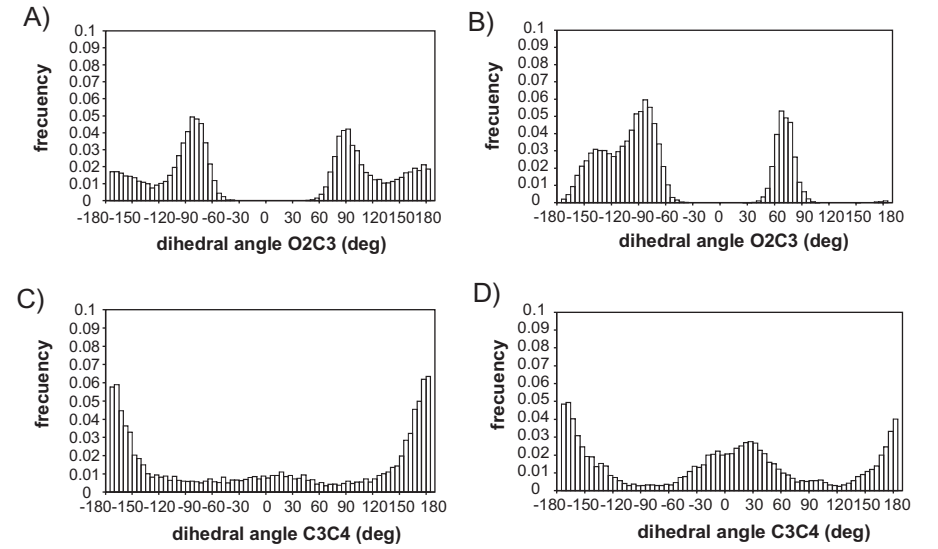

Figure 3.
Distribution of values obtained for the selected dihedral angles using the modified PCFF. Graphs A and C: PGA; Graphs B and D: PLLA.

cefield reveal conformation angle frequency maxima (at −85° and 90°, and a less pronounced maximum at around 180°) being in reasonable agreement with the MP2 predictions. When considering the same torsion for PLLA, the quantum mechanically calculated torsion potential is not symmetric around 0°. It shows a high energy barrier at 0°, a shallow one at 130° and a very low one around −120°. On the other hand, the three minima of energy, are located at −75° (global minimum), 66° and −152° (this latter minimum is a very shallow minimum)[26] and again the dihedral angle frequency distributions should show an inverse behavior. The distribution of dihedral angles found for the PLLA models, created with COMPASS (cf. Figure 2B), is once more in considerable disagreement with these results, because it shows two maxima at 10° and 100°. PCFF forcefield performance is again much better for this torsion, showing three minima centered at −85°, 65° and −140° (see Figure 3B).

Concerning the second considered torsion, C3–C4, the MP2 calculations, carried out for a PGA fragment by Blomqvist et al., revealed a potential energy profile symmetric around 0°, with a main barrier at 100° and a global energy minimum at 180°.[26] The distribution of dihedral angles calculated in this work are quite similar for both forcefields (compare Figure 2C and 3C), although the distribution for PCFF shows more symmetry around 0°. However, the quantum mechanical study of the potential of the same torsion, for a PLLA fragment, revealed an energy barrier at −125°, a global minimum at 157°, and two local minima at 65° and −42°.[26] The distribution of dihedral angles for this torsion found in the COMPASS models shows a maximum at −90°, which is in disagreement with the previously mentioned results. On the contrary, the models generated using PCFF show a distribution of dihedral angles more in agreement with the quantum mechanical results, with a broad minimum between -120° and −60°, and maxima centered around −20°, 25° and 180°.

As a consequence of these results, the models, constructed and equilibrated using modified PCFF forcefield, were chosen for the evaluation of different static and dynamic properties to computationally characterize the *dry* state of these homopolyesters. Utilizing the same forcefield, these models were soaked with water, further equilibrated, and, likewise, analyzed to characterize different *wet* states of polyglycolide and poly(*L*-lactide). The interface models described below were also simulated employing the modified PCFF forcefield.

Sato et al.[28] reported the experimental variation of the specific volume with temperature for PLLA. Bulk models were further validated by comparison with these data. For this purpose, at least 160 ps of NPT–dynamics were performed, at different temperatures, for one of the constructed models for PLLA at 1 bar and at 2000 bar. The specific volume was then calculated as the inverse of the density at each temperature. The obtained values, together with the experimental ones from ref. [28], are plotted in Figure 4. Below the experimental melting point (441 K), the calculated values for the models are in good agreement with the experimentally obtained values and this is the temperature range most relevant for the typical applications of these materials. The most probable reason for the discordance at higher temperatures and higher pressure is that the simulated dynamics are not long enough to permit the characterization of this phase transition.

The bulk models are labeled PGA and PLLA for polyglycolide and poly(*L*-lactide) respectively, followed by a number indicating the percentage in weight of water in the corresponding model. For the simulation of hydrated systems, the contents of water were chosen to match experimentally characterized water-swollen stages in amorphous samples of the two homopolymers.[14,15] The first two water swollen systems for each polymer correspond to the first water content detected in the degradation experiments (PGA-1.7 and PLLA-2), and the last water content measured before weight loss

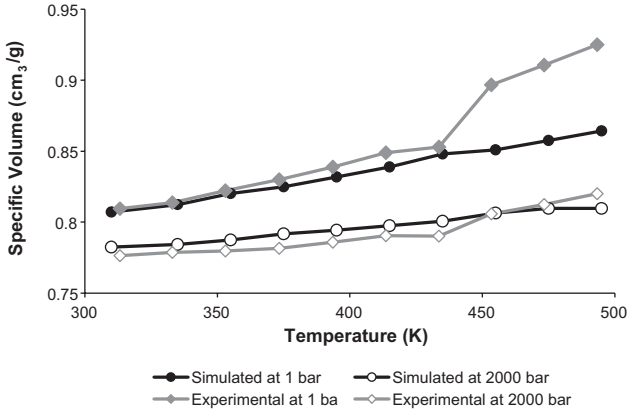

Figure 4.
Comparison between experimental and simulated specific volume as a function of temperature for PLLA. Experimental data from reference [28].

started (PGA-2.9 and PLLA-7). Afterwards, and for a better comparison between the two homopolymers, PGA with 7% water content by weight was simulated as well. In the experiments,[15] the weight loss has already started at this point.

The insertion of water was done stepwise using the Soak utility of the InsightII Software.[18,19] After soaking the models, a short NVT–MD, or when needed NPT–MD, was performed until the desired water content was reached. Then, the cells were subjected to further relaxation consisting of 20 ps NVT–MD and 1 ns NPT–MD ($p = 1$ bar, $T = 310$ K). In most cases, an additional 1 ns NPT–MD at $p = 1$ bar and $T = 310$ K was performed and used for the production of data.

Atomistic Simulations: Interface Models

The parameters for the constructed polymer–water interface models are shown in Table 2. They are labeled iPGA for polyglycolide and iPLLA for poly(*L*-lactide). The chains are identical to the ones used for the bulk models, made up of 50 repeat units per chain. The total number of atoms in the combined systems (polymer plus water) is 11988 for iPGA and 11528 for iPLLA.

For these models, first, a rectangular box containing the polymer was constructed and equilibrated. Then, the scaling of the forcefield and the annealing runs were performed in an analogous manner to the bulk models. The long equilibration runs performed next generally consisted of 1.5 ns NVT–MD at the experimental density and $T = 310$ K. Afterwards, a box with the same length in two of the dimensions (x, y) of the polymer box (see Table 2) was filled with an appropriate number of water molecules and equilibrated during 350 ps at a constant volume and $T = 310$ K. These boxes were constructed and equilibrated under two-dimensional periodic boundary conditions, where in the z–dimension of such a model, penalty surface potentials force the non-periodic (z) coordinates of the constituent atoms into a layer of thickness that results

Table 2.
General interface model parameters.

Polymer Packing	No. of chains/model	Initial dimensions of polymer layer (Å)	No. of water molecules/model	Initial dimensions of water layer (Å)
iPGA	30	$35 \times 35 \times 78.73$	968	$35 \times 35 \times 23.64$
iPLLA	30	$33 \times 33 \times 79.17$	980	$33 \times 33 \times 26.92$

from the other two box-lengths and the intended density of the system. In this way, splitting of bonds can be avoided after the subsequent combination of the polymer and the water boxes along the z–axis. The resulting polymer–water interface systems were then simulated under periodic boundary conditions in three dimensions. First, 20 ps NVT–MD with a time step of 0.1 fs were applied. Then, up to 4 ns NVT–MD with time step of 1 fs at $T = 310$ K were simulated. During these simulations, the temperature difference between the polymeric phase and the aqueous phase was checked. Temperature gaps can occur when the *Berendsen* thermostat is uniformly applied to models composed of two phases of different molecular mobility. However, this temperature difference, in the given case, was found to generally be about 10 K or lower, which is quite acceptable. Therefore, no separate atomic velocity scaling was applied to the polymer and the solvent parts of the respective models.

Quantum Chemical Calculations

Calculations were performed employing two different quantum chemical packages: TURBOMOLE V.5.8[29] and SPARTAN '04.[30] For computational reasons, the calculations were restricted to the gas phase and the size of the studied systems was limited to oligomers constituted of three repeat units of glycolyl (GG) and three repeat units of lactyl (LL), (see Figure 5 for their chemical structure and chirality). For hydrolysis in aqueous media, there is experimental evidence of the involvement of at least two water molecules in the reaction: while the first water molecule acts as a nucleophile, the second one acts as a general base abstracting a proton from the former one.[31] Theoretical computations have shown that the models in which this second water molecule is taken into account are more realistic and provide energy profiles in agreement with experiments.[32,33] Furthermore, in our previous investigation,[17] we found that in the less water swollen models, molecules of water are, on average, clustering in couples. Therefore, we investigated the water-assisted hydrolysis for these systems. For the *L*–lactyl containing trimer, the nucleophilic water can approach from two sides, the side where the methyl side group lies and the opposite one. The optimized structures, and corresponding structural data and energy barriers, obtained for the nucleophilic attack on the opposite side to the methyl group side are labeled LL-1, while the structures obtained for the attack on the methyl group side are labeled LL-2. Geometries at each stationary point were optimized without any constraints. The rate-controlling step in the reaction is the proton transfer between the two water molecules and the simultaneous nucleophilic attack of the first water molecule to the carbon atoms of the carbonyl group. Thus, in every instance, exclusively the reactants, the first transition state and the intermediate structures were calculated. The structures were optimized both at the HF/6-31G* and the B3LYP/6-31G* level of theory. For all optimized geometries, a frequency analysis was performed, using the AOFORCE module of TURBOMOLE to determine if the optimized geometry is a minimum or a first order saddle point in the energy surface.

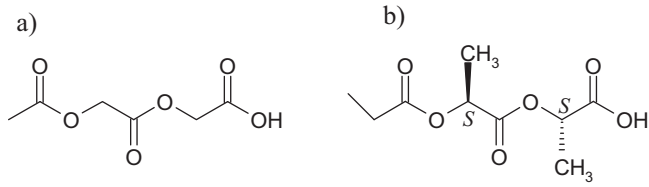

Figure 5.
Chemical composition of the investigated trimers (a) GG (b) LL.

Results and Discussion

As already explained in the introduction, the hydrolytic bulk degradation in amorphous and semi-crystalline polymers is mostly determined by the amorphous regions because transport of water molecules is only possible there. This fact makes it reasonable to perform atomistic MD-simulations on the amorphous phase of polymers like PGA or PLLA. The resulting findings are discussed below. Since PGA and PLLA usually show some crystallinity, with typical degrees of crystallinity being about 40%, it makes sense to also briefly mention possible effects of hydrolytic degradation conditions on the crystalline phase. Normally, as a general trend, an increase in crystallinity is observed as the hydrolytic degradation is proceeding. This effect is, in the simplest case, solely caused by the ongoing removal of already degraded low-molecular weight material from the amorphous regions. In addition, other changes in the crystalline phase are possible. Since water can not soak most polymer crystals, possible degradation (e.g. decrease in size) of individual crystallites, which normally have a size of several nanometres, will happen via a surface degrading process, i.e. detaching easily accessible lattice planes. A competing process of crystal growth, connected with the general decrease of molecular weight of the remaining polymer chain segments, can take place as well. Atomistic molecular modelling is, however, not the optimum tool to address these questions. Therefore, in the future, combined approaches of molecular modelling and wide angle X-ray scattering (WAXS) shall be used to get a more complete overview.

Polymer–Water Interface

Snapshots of the constructed models for the interaction between PGA and PLLA with water after 4 ns NPT–MD simulation are shown in Figure 6a and 7a, respectively. Positioned below each snapshot, Figure 6b and 7b, the corresponding normalized concentration profile for both the polymer (light gray line) and the water (black line)

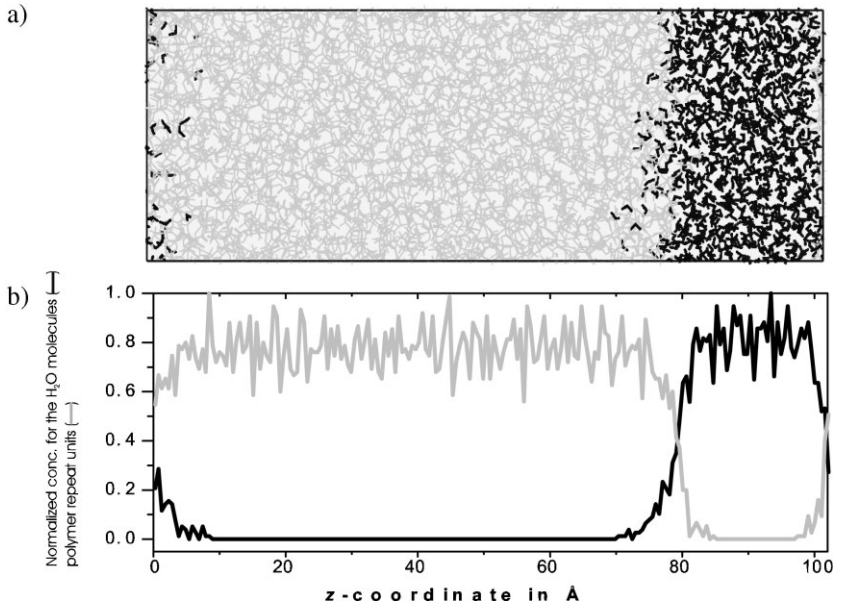

Figure 6.
Snapshot of the interface model iPGA (a) and normalized concentration profile (b). Polymer = light gray, water = black.

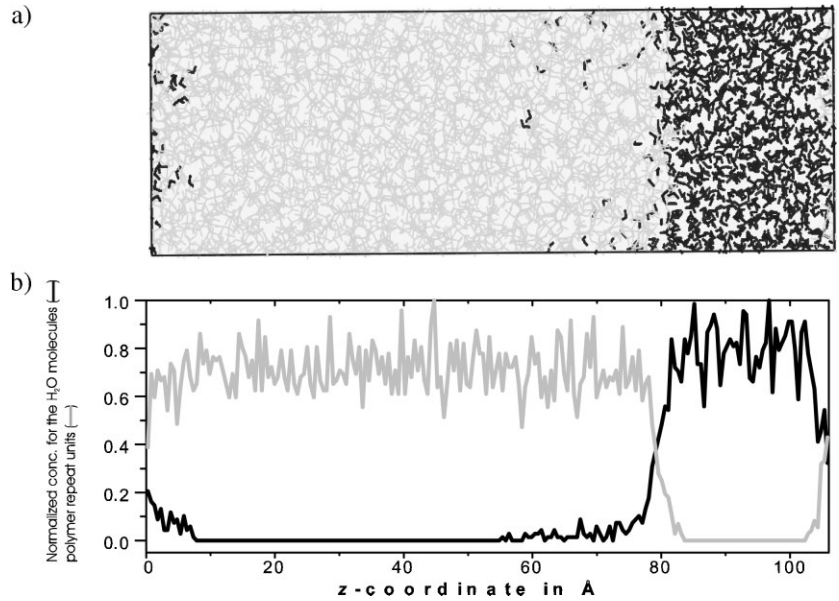

Figure 7.
Snapshot of the interface model iPLLA (a) and normalized concentration profile (b). Polymer = light gray, water = black.

in the model can be found. The normalized concentration profile describes the concentration of water molecules or polymeric repeat units relative to the maximum concentration. A certain number of water molecules penetrated both polymeric matrices after dynamics simulations longer than 4 ns. However, the water molecules that managed to penetrate the PLLA matrix moved further than the water molecules in PGA. This is consistent with the higher calculated diffusivity of water in PLLA (see below). At the same time, PGA seems to have a closer contact with the aqueous phase: although the water molecules did not diffuse too far into the PGA matrix, they seem to be more mingled with the polymer in the vicinity of the interface. Both observed trends were confirmed by the bulk model simulations discussed below.

Study of the Bulk of Dry and Hydrated Polymers. Interaction with Water

Permeability – in terms of a solution–diffusion mechanism – is used to describe the transport of a gas, vapor or liquid through a dense, non-porous polymer, and this mechanism can thus also be employed to explain the water uptake in the given case. The permeability coefficient is obtained as the product of the diffusion coefficient multiplied by the solubility. Therefore, properties, related to the diffusion and the solubility of water in the polymers, were analyzed in the simulated cells as discussed below.

In polymers with similar chemical structure, the diffusion of a penetrant inside a dense matrix depends primarily on the amount and topology of the free volume existing in the polymer. Nevertheless, the mobility of the polymeric chains has to be considered as well, because the chain motions permit the redistribution of the free volume, consequently contributing to the jumps of a penetrant molecule (here water) from one site to another.[34,35]

Hence, we have investigated the free volume in the *dry* models, in addition to the models with different levels of hydration. To quantitatively characterize the free

volume, a snapshot was selected for each validated model. The atoms of the models were represented by atomic hard spheres, employing the van der Waals atomic radii of the respective atoms (1.55 Å for C, 1.35 Å for O and 1.10 Å for H). Next, a three dimensional cubic grid with a grid side of 0.7 Å was placed over the model. At each grid point, it was tested whether a hard sphere with a certain radius –corresponding to a specific probe molecule – overlapped with the hard spheres representing the atoms of the polymer. In the cases where overlap existed, these points were considered to belong to the polymeric matrix and were considered *occupied*. The remaining grid points, where no overlap was found, were considered *free*. The grid points tagged as *free*, with the corresponding lattice cube of $(0.7\ \text{Å})^3$ surrounding them, are named free volume elements (FVE). The FVE shape the free volume accessible to the probe molecule utilized in each particular case. In order to examine the free accessible volume in the hydrated cells, the water molecules were removed prior to the free volume analysis.

The fractional free accessible volume (FAV) for a probe molecule corresponds to the ratio of *free* grid points to total grid points, as shown in Table 3 for two different probe molecules: water, with a radius of 1.4 Å, and orthopositronium (o-Ps), with a radius of 1.1 Å. In order to determine the total fractional free volume (FFV) (also shown in Table 3), the free volume accessible for probe molecules with a radii of 0.4 and and 0.25 Å^3 was calculated (for these calculations, the grid size was reduced to 0.4 Å and 0.25 Å, respectively). Afterwards, the FFV was calculated, by extrapolation to a radius of 0.0 Å of the quadratic regression line of the obtained FAV, for the different probe molecules. This FFV is comparable to subtracting the volume occupied by the atoms of the polymer from the overall volume of the model. The values were averaged over the three models existing for each system.

Table 3 shows that PLLA has a higher overall fractional free volume and fractional free volume accessible to a water molecule than PGA. This difference is sizeable in the water-free models – where the fractional free volume accessible to water is more than nine times larger in PLLA than in PGA – and considerably smaller in the hydrated models. This finding implies looser chain packing for PLLA, particularly in the *dry* state. The difference in free volume is primarily connected with differences in the contents of larger free volume elements, i.e. free volume accessible to a water molecule. This can be seen in more detail via accessible free volume distribution histograms which have been published elsewhere.[17] Here, Figure 8 shows only a comparison between these graphs for the cases of 7% water contents (this graph was not shown in ref. 16 for PGA). It is clearly visible that PLLA not only has a higher overall amount of water accessible free volume, but that its respective free volume distribution histograms also extend to larger hole radii than for those of PGA.

Table 3.
Total fractional accessible volume (FAV) calculated for probe molecules with different radius and volumetric swelling undergone by the models at the different simulated hydration stages.

System	Fractional accessible volume (FAV) for probes with radii R_i (Å)			Volumetric swelling $\Delta V = V_{wet}/V_{dry}$
	1.40 (H_2O)	1.10 (o-Ps)	0.00 (FFV)	
PGA-0	0.0012	0.0128	0.5947	–
PGA-1.7	0.0112	0.0348	0.5938	1.020 ± 0.003
PGA-2.9	0.0232	0.0532	0.5942	1.034 ± 0.002
PGA-7	0.0777	0.1206	0.6041	1.092 ± 0.003
PLLA-0	0.0109	0.0490	0.6349	–
PLLA-2	0.0266	0.0722	0.6361	1.017 ± 0.002
PLLA-7	0.0931	0.1437	0.6400	1.070 ± 0.002

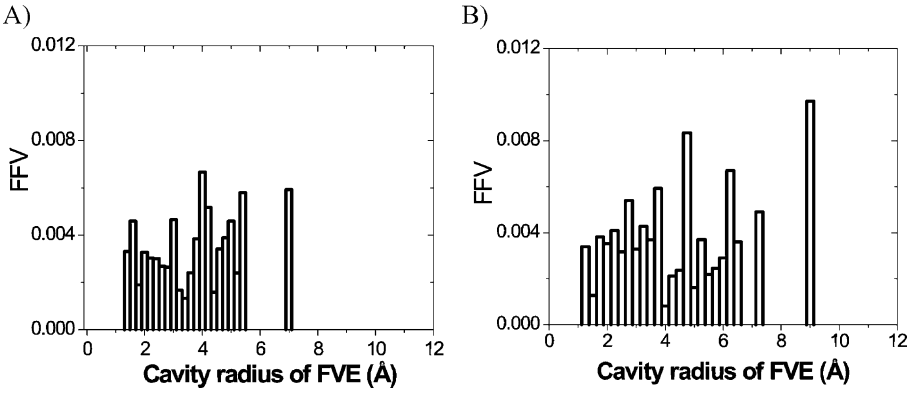

Figure 8.
Distribution of free volume elements (FVE) accessible for H_2O for the models containing 7% of water contents in weight. A: PGA, B: PLLA.

In order to explain these differences concerning the free volume, the torsional flexibility of the segments of the chains was assessed via systematic conformational scans. Values of potential energy were computed by rotating the molecule around two adjacent backbone bonds in steps of 1 °. At each conformation, an energy minimization of 300 iterations was performed, constraining the selected dihedral to maintain its value fixed during the minimization. For the rotation around the C3–C4 bond (see Figure 1b for the labeling of the atoms), relatively small torsional barriers were found, approx. 8–13 kJ/mol. The profile for the torsion potential is very similar for the two kinds of fragments, glycolyl and *L*-lactyl units. This indicates that the introduction of the pendant methyl group does not create a big steric strain on the adjacent carbonyl group – the one corresponding to the C4 atom. However, a large steric strain on the methyl group with the carbonyl group in the β position – the one corresponding to the C1 atom – was found when the rotation around the O2–C3 bond was investigated. The definition of this rotation is shown in Figure 1a. For this rotation, the glycolyl fragment presents only one high torsional barrier at 0 °, of about 45.4 kJ/mol (see Figure 9). The *L*-lactyl fragment, however, presents two high

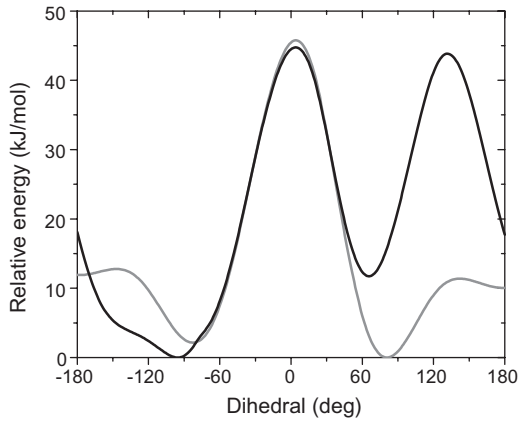

Figure 9.
Torsion potential for the O2–C3 dihedral angle: R = –H (▬), R = $-CH_3$ (▬).

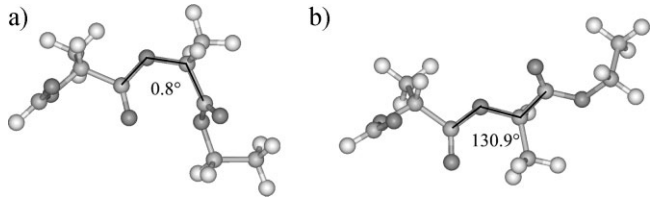

Figure 10.
Illustration of the molecular geometry corresponding to the two torsional barriers.

torsional barriers: one of about 44.3 kJ/mol at 0 ° and a second one of 43.6 kJ/mol at 130 °. The molecular geometries corresponding to the two torsional barriers are shown in Figure 10. The barrier around 0 °corresponds to the eclipsed conformation between the carbonyl in β and the rest of the backbone, and thus, it is present for the glycolyl and the *L*-lactyl fragments (see Figure 10a). The torsional barrier at 130 °corresponds to the eclipsed conformation between the carbonyl in β and the pendant methyl group present only in the *L*-lactyl unit (see Figure 10b). The existence of this second high torsional barrier implies a higher backbone conformational stiffness for the *L*-lactyl fragments than for the glycolyl fragments. This higher conformational stiffness is likely the major reason for the differences in free volume between the two polymers. It makes *L*-lactyl rich polymer chain segment packing more difficult, thus leading to a higher fractional free volume contents in this polymer. Similar effects have also been previously found, e.g. for polyimides used in gas separation.[36]

The observed differences between PGA and PLLA in the redistributions of free volume when water molecules are inserted are connected to the higher volumetric swelling undergone by the polyglycolide models in comparison to the poly(*L*-lactide) models (see Table 3). The volumetric swelling was obtained as an average of the values computed for the three independent models built for each polymer. For each model, ΔV was determined as the quotient of the volume of the water containing models, V_{wet}, and the volume of the *dry* models, V_{dry}. Both V_{wet} and V_{dry} were calculated as the average volume of the corresponding model during the data production run. Because more free volume accessible to water is available in PLLA, the insertion of a certain amount of water implies less dilation of the systems in comparison to PGA, where less initial FVA can be filled by the water molecules. In addition, the stronger interaction of water with glycolyl units and *L*-lactyl units prevails over the conformational stiffness in the hydrated systems: as soon as the free volume accessible to water excesses a critical limit, the differences in the local conformation stiffness on the repeat units are no longer decisive in the specific chain segment packing order of the polymer.

Figure 11 shows the mean square displacement for the polymer atoms in the dry state (A) and in the water-swollen models (B and C). The mean square displacement, MSD, gives a measure of the self-diffusion of the polymeric chain-segments. This was evaluated during 500 ps NPT–MD in the first case, and 1 ns NPT–MD in the latter one, with snapshots taken every 1000 steps. The MSD is obtained as $s(t) = \left\langle |r(t) - r(0)|^2 \right\rangle$, where $r(t)$–$r(0)$ is the distance traveled by a particle over a time interval t. The brackets indicate an average for all atoms at all possible time origins. The mobility of the chains increases for both systems with hydration (higher slope). However, the mobility of PLLA is higher in all systems. Evaluating Figure 11, one should recognize that MSD-curves over roughly the last 20% of the averaged time are typically of low statistical quality, and in this region, are often influenced by systematic errors.

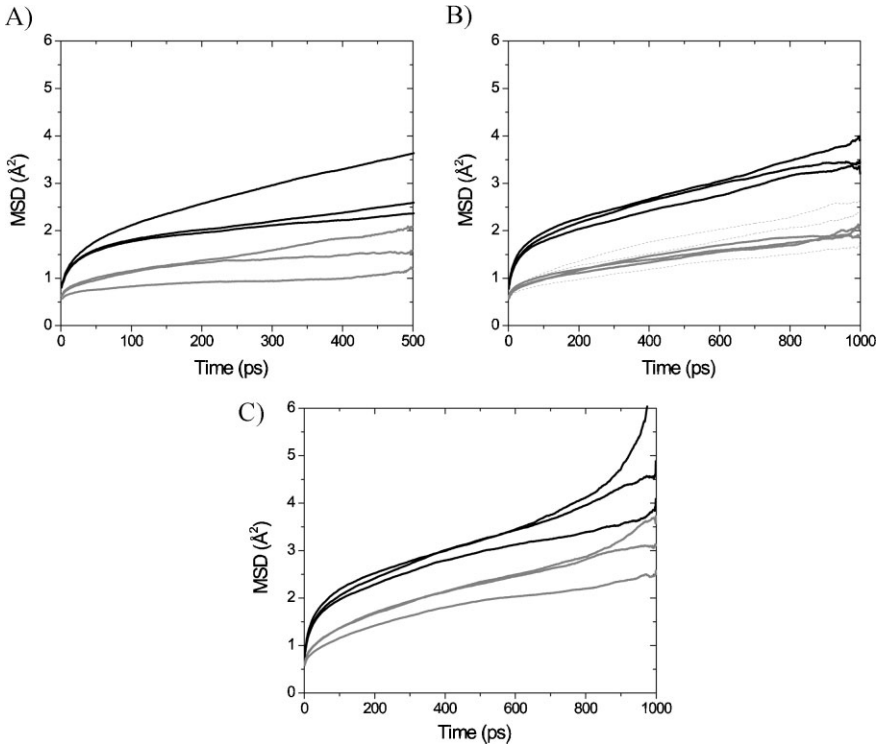

Figure 11.
Mean square displacement vs. time for the diffusion of atoms of the polymer. A: PGA-0 (—) and PLLA-0 (—), B: PGA-1.7 (—), PGA-2.9 (- - -) and PLLA-2 (—), C: PGA-7 (—) and PLLA-7 (—).

The constants of diffusion for water through the polymeric matrixes can be obtained, in principle, from the MSD of the water molecules from the evaluation of the so-called Einstein equation:

$$D = \left\langle |r(t) - r(0)|^2 \right\rangle \Big/ 6t$$

This equation can only be used with full confidence in the regime of normal diffusion, since it assumes a random walk for each simulated particle. The realm of normal diffusion is reached when the slope of the function $\log[s(t)] = f[\log(t)]$ equals 1. For the diffusion of water through the polyesters studied here, the normal diffusive regime was not reached during the data production runs, and thus the slope of this function is lower than 1. Consequently, the values obtained from the MSD for the diffusion coefficient of water in the polymers can only be used as trend indicators and are shown in Table 4. The diffusion of water was higher in PLLA than in PGA, as expected from the higher free volume accessible to water and a higher self-diffusion of this polymer. This result is in agreement with experimentally obtained diffusion coefficients published by Ion et al.,[37] which have a higher value for water in PLLA than in PGA.

The Hildebrand's solubility parameter,[38] δ, is an indication of the interatomic interactions in the polymer matrix, and is of great value in order to understand the solubility of two substances. Solubility is greater between substances with similar interatomic forces, that is, between substances with closer values of the solubility parameters. The solubility parameters can be calculated for the simulated models as the square root of the cohesive energy

Table 4.
Calculated constants of diffusion – obtained directly from the MSD of the water molecules in the models – and solubility parameters.

System	Simulated constant of diffusion for water (10^{-6} cm^2s^{-1})	Solubility parameter δ $(J/cm^3)^{1/2}$		Hydrogen bond energy (kJ/mol)
		In presence of water[a)]	After water removal	
PGA-0	–	31.9 ± 0.3	–	–
PGA-1.7	5.07 ± 1.00	32.7 ± 0.2	31.3 ± 0.2	125.6 ± 7.7
PGA-2.9	5.69 ± 2.00	33.0 ± 0.2	30.8 ± 0.2	145.2 ± 51.7
PGA-7	10.76 ± 1.49	33.9 ± 0.5	28.9 ± 0.4	471.4 ± 32.3
PLLA-0	–	23.3 ± 0.1	–	–
PLLA-2	5.94 ± 2.24	24.2 ± 0.2	22.6 ± 0.2	119.7 ± 19.3
PLLA-7	17.27 ± 0.60	26.3 ± 0.1	21.3 ± 0.1	337.4 ± 58.1

[a)] PGA-0 and PLLA-0 contain no water (reference models).

density, which is defined in atomistic modeling as the increase in energy per mole of material if all intermolecular forces are eliminated. The values obtained for PGA and PLLA are listed in Table 4. The solubility parameters were calculated as an average of the three models for each polymer at each hydration stage. For PLLA, the calculated solubility parameter, using a group contribution method, was found to be 22.7 $(J/cm^3)^{1/2}$,[39] which is quite similar to the observed value shown in Table 4. In comparison to PLLA, the δ of PGA is closer to that of water, 47.9 7 $(J/cm^3)^{1/2}$, thus indicating a higher solubility of water in PGA. The solubility parameter, when calculated after removal of the water in the models (see Table 4), decreases with a higher degree of hydration, due to the diminution of cohesion in the polymeric matrix in the presence of water. This result shows coherence with the experimentally measured solubility coefficient, which is higher for water in PGA, as well as with higher hydrophilicity, determined in terms of surface tension and contact angle measures.[39]

As mentioned above, it was experimentally established that polyglycolide undergoes a much faster water uptake and degradation than poly(*L*-lactide) for both semicrystalline and amorphous (obtained by quenching) samples of the polymer. Since the faster measured water uptake for PGA means higher water permeability, and because the water diffusion is lower for PGA than for PLLA, while the trend for the solubility is opposite, it can be concluded that the higher solubility of water in PGA is overcompensating for the lower water diffusivity in this polymer. This behavior can easily be understood because the only major structural difference between PGA and PLLA is the presence of an additional methyl group in PLLA, which leads to a lower density of polar groups and thus a lower level of polar interaction energy density. For that reason, the energetic interactions with the water molecules are weaker for PLLA than for PGA, which explains the differences in water solubility and eventually different levels of water uptake.

The stronger interaction between water and PGA, in comparison to PLLA, is also reflected in the higher number of hydrogen bonding interactions existing between water and PGA compared to the lower number of interactions found between water and PLLA (cf. Table 4). The calculation of the hydrogen bond energy between water and polymer was carried out (for the models originally equilibrated with the modified PCFF) using the AMBER forcefield,[40] because the modified PCFF does not include a specific term for the hydrogen bond energy. The AMBER forcefield includes a '10–12' hydrogen bond potential. To obtain this contribution to the energy of the system, single point energy calculations using AMBER were performed. The energies were averaged over three independent models in each case using a single equilibrated

structure for each of them (explaining the large standard deviations attached to the computed values).

Transition States and Activation Energies

Using structural information for the transition states of the water-assisted hydrolysis of similar esters, e.g. ethyl acetate,[41] the transition state, TS_1, for the first step in the hydrolysis was found for the selected trimers at HF/6-31G*. These structures were further optimized at B3LYP/6-31G* level. The TS_1 found at both levels of calculation for all systems are characterized by a tetrahedral carbonyl carbon, as shown by the measured values for the Oc–C1–O1 angle (cf. Table 5). However, the steric hindrance by the methyl group results in an Oc–C1–O1 angle lower than the tetrahedral angle when the water attacks from the methyl group side, LL-2.

In the three calculated transition states, a six-membered ring structure involving the carbonyl atoms and the two water molecules was found: C1–O1–H1b–O2–H2a–Oc (see Figure 12). The distance between the carbonyl carbon, C1, and the oxygen of the water acting as a nucleophile, O1, is 1.7 Å for the *L*-lactyl containing trimers, LL-1 and LL-2, coincidentally the same distance calculated for water-assisted hydrolysis of ethyl acetate.[41] For the glycolyl trimer, GG, this distance is somewhat shorter, 1.6 Å, and equal to the one calculated for the water-assisted hydrolysis of fluoro and chloro substituted ethyl acetate, where the carbonyl carbon is more electrophilic. This difference can be attributed to the positive inductive effect (electron releasing) of the methyl group present in the *L*-lactyl units. Moreover, the existence of the additional methyl group in the *L*-lactyl units has a steric effect, as well. This can be seen in the geometry of the transition states, where the chain is bent more in LL than in GG, due to the steric repulsion with the nucleophilic water molecule. The C2–C1–O1 and the C2–C1–O angles show values of 99.8° and 107.3° for GG, but 104.8° and 112.2° for LL-1 and 102.3° and 108.0° for LL-2, respectively.

The energy profiles for the rate limiting step of the water-assisted hydrolysis of the trimers are shown in Figure 13 and 14, for both levels of calculation. The corresponding energy barriers are listed in Table 6. At both levels of computation, the lowest barrier was found for the trimer constituted by glycolyl units, GG. This shows agreement with experimental findings in copolymers

Table 5.
Characteristic geometrical parameters of the calculated transition states at B3LYP/6-31G* computational level.

Parameter[b)]	reactants			TS_1			intermediate		
	GG	LL-1	LL-2	GG	LL-1	LL-2	GG	LL-1	LL-2
distance (Å)									
C1–O1	3.1	2.9	3.7	1.6	1.7	1.7	1.4	1.4	1.4
O1–H1a	0.97	0.97	0.97	0.98	0.99	0.97	0.98	0.98	0.97
O2–H1b	1.9	1.9	2.0	1.2	1.2	1.2	0.97	0.97	0.97
O2–H2a	0.97	0.97	0.97	1.1	1.1	1.2	1.7	1.7	1.8
Oc–H2a	4.1	2.1	3.8	1.4	1.4	1.3	0.99	0.99	0.99
***angle* (degree)**									
C1–O1–H1b	85.4	80.9	78.4	98.5	97.9	98.4	98.1	92.5	100.4
O1–H1b–O2	160.4	161.7	152.9	156.9	157.5	156.6	127.7	92.6	133.2
H1b–O2–H2a	97.1	96.8	83.7	86.1	85.7	84.4	89.9	100.7	87.7
O2–H2a–Oc	148.9	148.7	154.7	152.6	154.0	157.2	162.0	169.0	161.0
H2a–Oc–C1	113.8	105.7	142.1	105.5	105.4	107.6	107.4	107.5	106.8
Oc–C1–O1	102.8	102.8	54.3	110.4	109.8	106.9	112.7	113.7	112.3
C2–C1–O1	74.0	88.7	80.3	99.8	104.8	102.3	104.2	112.7	110.1
C2–C1–O	110.9	119.2	110.9	107.3	112.2	108.0	106.5	108.4	111.1
***dihedral* (degree)**									
O1–Oc–C1–O	101.3	−90.5	134.3	116.9	−112.8	115.5	123.1	−117.9	115.2

b) Atom labels shown in Figure 12.

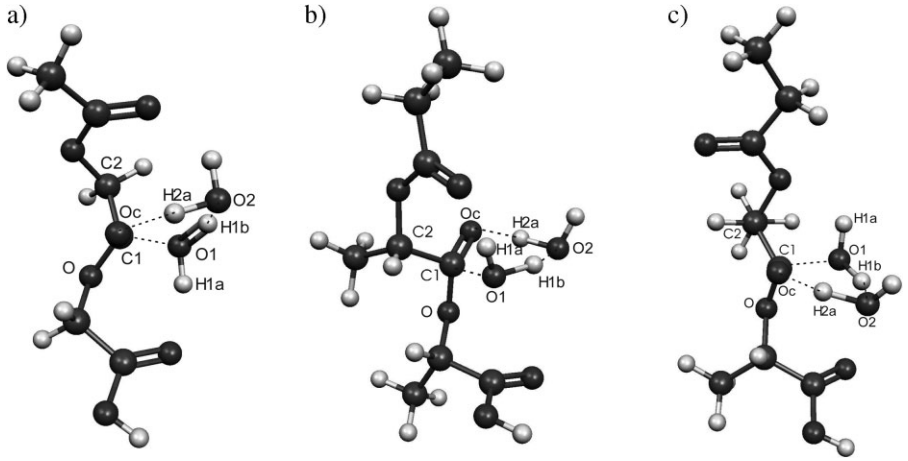

Figure 12.
Optimized structures for the transition states TS_1 calculated at B3LYP/6-31G* computational level: (a) GG (b) LL-1 (c) LL-2.

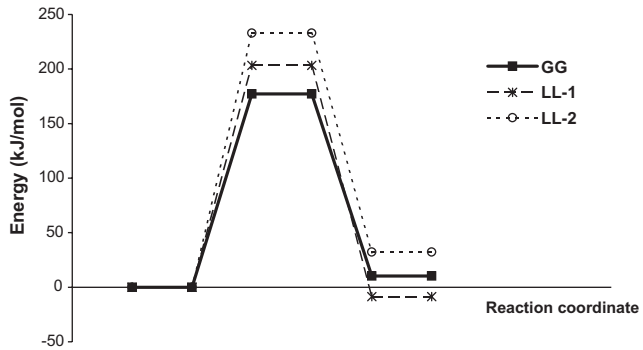

Figure 13.
Energy profile for the first step of the hydrolysis at HF/6-31G* computational level.

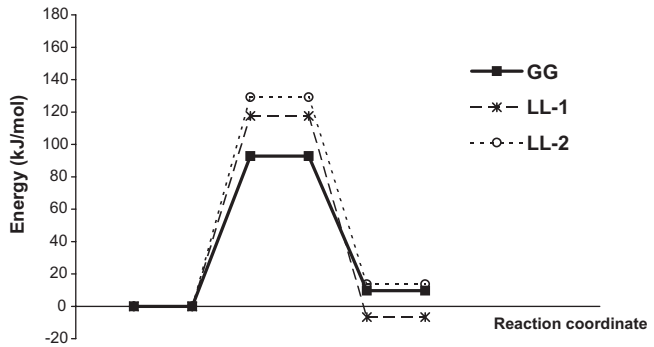

Figure 14.
Energy profile for the first step of the hydrolysis at B3LYP/6-31G* computational level.

Table 6.
Energy barriers for the different investigated structures at HF/6-31G* and B3LYP/6-31G* computational levels.

System	ΔE (kJ/mol)	
	HF/6-31G*	B3LYP/6-31G*
GG	177.14	92.83
LL-1	203.33	117.52
LL-2	232.94	129.19

containing glycolyl and *L*-lactyl units, where the cleavage occurred preferentially at the glycolide linkages.[42] In addition, experiments with different poly[(*rac*-lactide)–*co*–glycolide)]s established faster hydrolytic cleavage with higher contents of glycoly units.[43] This higher activation energy found for *L*-lactyl units, compared to glycolyl ones, is explained by both the electronic and steric effects of the methyl group present in *L*-lactyl units. A lower electrophilic character of the carbonyl carbon in the lactyl units results from the electron releasing effect of the methyl group. At the same time, the presence of this methyl as a pendant group hinders the nucleophilic attack of the oxygen of the water on the carbonyl atom. Also, at both levels of computation, the energy barrier is higher for the nucleophilic attack on the methyl group side (LL-2), where steric hindrance to the attack is higher.

Conclusion

A higher solubility of water in PGA than in PLLA is responsible for the higher water uptake observed in the degradation experiments, overcompensating the higher diffusivity of water through PLLA. This higher affinity of water for PGA is related with the higher density of polar groups existing in PGA, due to the absence of the methyl group that PLLA has as a side chain. The first moments of contact between the polymeric and the aqueous phase were investigated employing atomistic interface models, which also showed faster water diffusion through PLLA. Quantum mechanical calculations, of the first step in the water-assisted hydrolysis of trimers constituted of glycolyl and *L*-lactyl units, revealed a more favorable hydrolysis of glycolyl units than of *L*-lactyl units. A lower energy barrier was found for the scission of the glycolyl units in compared to the scission of the *L*-lactyl units. This is due to the electronic and steric influence of the presence of the additional methyl group in *L*-lactyl units.

In summary, the faster experimentally observed degradation of polyglycolide over poly(*L*-lactide) is caused by a higher water solubility and preferential hydrolysis of glycolyl units over *L*-lactyl units.

Acknowledgements: This work was financially partially supported by the European Community (Project: NMP3-CT-2005-013644 ''MULTIMATDESIGN''). The authors also want to thank the German Academic Exchange Service (DAAD/RISE program) for support.

[1] P. A. Gunatillake, R. Adhikari, *Eur. Cell. Mater.* **2003**, *5*, 1.
[2] M. Kellomäki, H. Niiranen, K. Puumanen, N. Ashammakhi, T. Waris, P. Törmälä, *Biomaterials* **2000**, *21*, 2495.
[3] J. M. Anderson, M. S. Shive, *Adv. Drug Delivery. Rev.* **1997**, *28*, 5.
[4] D. W. Hutmacher, *Biomaterials* **2000**, *21*, 2529.
[5] J. C. Middleton, A. J. Tipton, *Biomaterials* **2000**, *21*, 2335.
[6] J. Panyam, V. Labhasetwar, *Adv. Drug Delivery. Rev.* **2003**, *55*, 329.
[7] A. Lendlein, S. Kelch, *Science.* **2002**, *296*, 1673.
[8] N.-Y. Choi, S. Kelch, A. Lendlein, *Adv. Eng. Mater.* **2006**, *8*, 439.
[9] W. Heidemann, J. H. Fischer, J. Koebke, C. Bussmann, K. L. Gerlach, *Mund Kiefer GesichtsChir.* **2003**, *7*, 283.
[10] G. E. Zaikov, U. S. Livshits, *Pharm. Chem. J.* **1984**, *18*, 288.
[11] M. Vert, S. Li, H. Garreau, J. Mauduit, M. Boustta, *Angew. Makromol. Chem.* **1997**, *247*, 239.
[12] K. Rezwan, Q. Z. Chen, J. J. Blaker, A. R. Boccaccini, *Biomaterials* **2006**, *27*, 3413.
[13] F. Alexis, *Polym. Int.* **2005**, *54*, 36.
[14] S. Li, H. Garreau, M. Vert, *J. Mater. Sci. – Mater. Med.* **1990**, *1*, 206.
[15] S. Hurrel, R. E. Cameron, *Biomaterials* **2002**, *23*, 2401.
[16] S. Li, *J. Biomed. Mater. Res.* **1999**, *48*, 342.
[17] M. Entrialgo-Castaño, A. Lendlein, D. Hofmann, *Adv. Eng. Mater.* **2006**, *8*, 434.

[18] Molecular Simulations Inc., San Diego, CA, *Polymer User Guide, Amorphous Cell Section, Version 4.0.0.p+* **1999**.
[19] Molecular Simulations Inc. San Diego, CA, *Discover User Guide, Versión 2.9.8./96.0/4.0.0., Forcefield Simulations* **1996**.
[20] D. Hofmann, L. Fritz, J. Ulbrich, C. Schepers, M. Böhning, *Macromol. Theory Simul.* **2000**, *9*, 293.
[21] H. J. C. Berendsen, J. P. M. Postma, W. F. van Gusteren, A. DiNola, J. R. Haak, *J. Chem. Phys.* **1984**, *81*, 3684.
[22] U. Gaur, S.-F. Lau, B. B. Wunderlich, B. Wunderlich, *J. Phys. Chem. Ref. Data* **1983**, *12*, 65.
[23] K. Chujo, H. Kobayashi, J. Suzuki, S. Tokuhara, M. Tanabe, *Makromol. Chem.* **1967**, *100*, 262.
[24] K. van de Velde, P. Kiekens, *Polym. Test.* **2002**, *21*, 433.
[25] H. Sun, D. Rigby, *Spectrochim. Acta* **1997**, *53A*, 1301.
[26] J. Blomqvist, B. Mannfors, L.-O. Pietilä, *J. Mol. Struct. (Teochem)* **2000**, *531*, 359.
[27] J. Blomqvist, L. Ahjopalo, B. Mannfors, L.-O. Pietilä, *J. Mol. Struct. (Teochem)* **1999**, *488*, 247.
[28] Y. Sato, K. Inohara, S. Takishima, H. Masuoka, M. Imaizumi, H. Yamamoto, M. Takasugi, *Polym. Eng. Sci.* **2000**, *40*, 2602.
[29] R. Alrichs, M. Bär, M. Häser, H. Horn, C. Kölmel, *Chem. Phys. Letters* **1989**, *162*, 165.
[30] *Spartan '04 Windows. Tutorial and User's Guide*, Wavefunction, Inc. Irvine, USA **2001–2004**.
[31] R. S. Brown, A. J. Bennet, H. Slebocka-Tilk, *Acc. Chem. Res.* **1992**, *25*, 481.
[32] R. Kallies, R. Mitzner, *J. Mol. Model.* **1998**, *4*, 183.
[33] M. F. Lensink, J. Mavri, H. J. C. Berendsen, *J. Comput. Chem.* **1999**, *20*, 886.
[34] H. Takeuchi, K. Okazaki, *J. Chem. Phys.* **1990**, *92*, 5643.
[35] K. Choi, W. H. Jo, *Macromolecules* **1995**, *28*, 8598.
[36] S. A. Stern, *J. Membr. Sci.* **1994**, *94*, 1.
[37] J.-S. Ion, H.-W. Jung, M.-N. Kim, E.-S. Park, *J. Appl. Polym. Sci.* **1998**, *77*, 1716.
[38] J. H. Hildebrand, *J. Am. Chem. Soc.* **1929**, *51*, 66.
[39] R. Shogren, *J. Environ. Polym. Degr.* **1997**, *5*, 91.
[40] S. J. Weiner, P. A. Kollman, D. A. Case, U. Chandra, C. Ghio, G. Alagona, S. Profeta, Jr., P. Weiner, *J. Am. Chem. Soc.* **1984**, *106*, 765.
[41] G. Schmeer, P. Sturm, *Phys. Chem. Chem. Phys.* **1999**, *1*, 1025.
[42] F. Alexis, S. Venkatraman, S. K. Rath, L.-H. Gan, *J. Appl. Polym. Sci.* **2006**, *102*, 3111.
[43] X. S. Wu, N. Wang, *J. Biomater. Sci. Polymer Edn.* **2001**, *12*, 21.

